Figures and figure supplements

Folding of cohesin's coiled coil is important for Scc2/4-induced association with chromosomes

Naomi J Petela *et al*

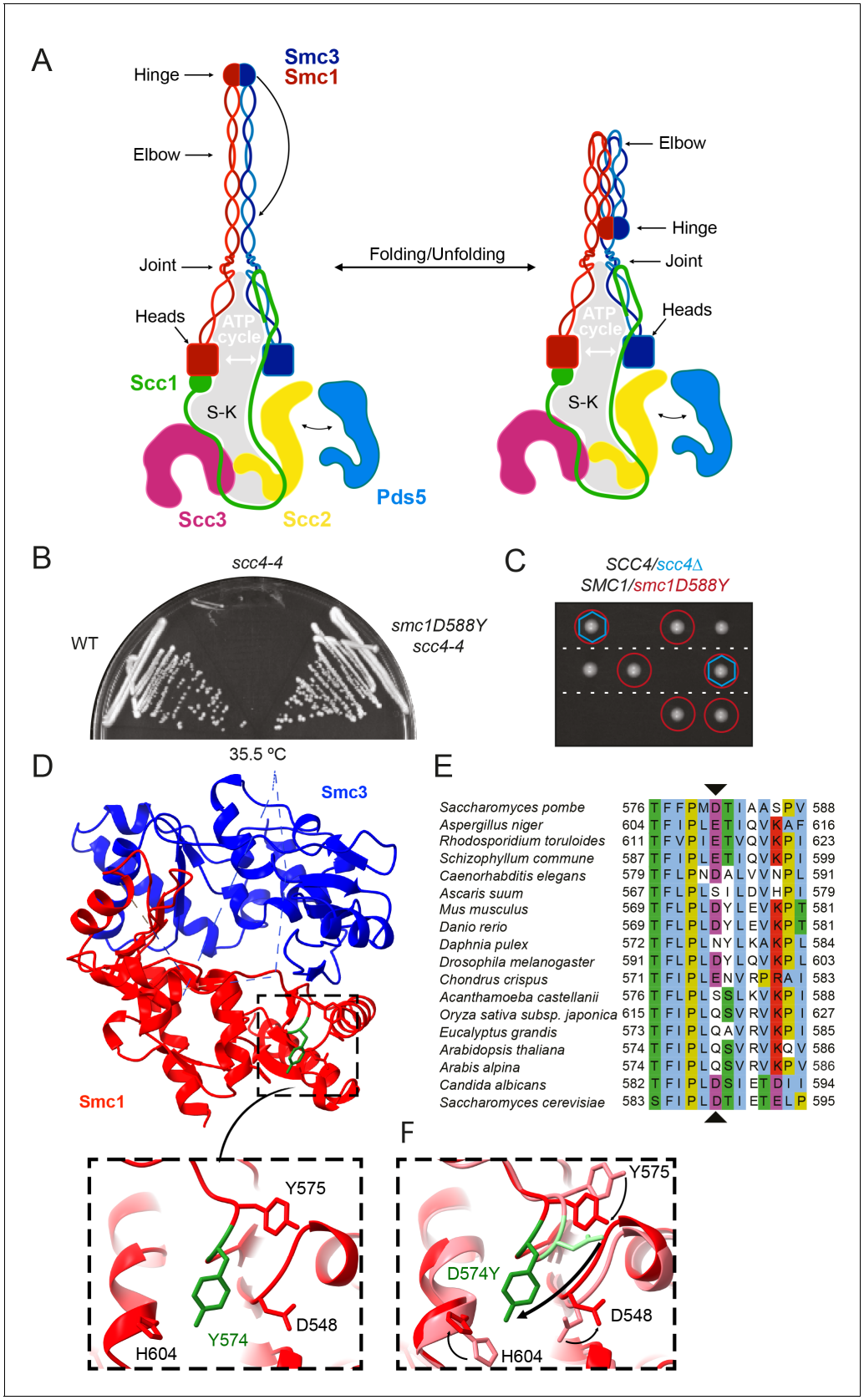

Figure 1. A mutation in the hinge domain of Smc1 restores viability in the absence of Scc4. (**A**) Schematic representation of *Saccharomycescerevisiae* cohesin complex and its folding cycle. (**B**) Comparison of growth of wild-type (WT), *scc4-4,* and *scc4-4 smc1D588Y* strains at 35.5˚C (K699, K8326,

Figure 1 continued on next page

Figure 1 continued

K19813). (**C**) Tetrad dissection of diploid strains containing *SCC4/scc4Δ SMC1/smc1D588Y* grown at 30°C. Spores expressing *smc1D588Y* are circled in red, and spores that lack Scc4 are indicated with blue hexagons. (**D**) Structure of the mouse Smc3-Smc1D574Y hinge domain (PDB: 7DG5). (**E**) Multiple sequence alignment indicating conservation of Smc1D588. (**F**) Structural superposition of the WT hinge and the D574Y mutant hinge. Tyr574 swings out relative to the position of D574 with a concomitant local conformational change of the mutated loop.

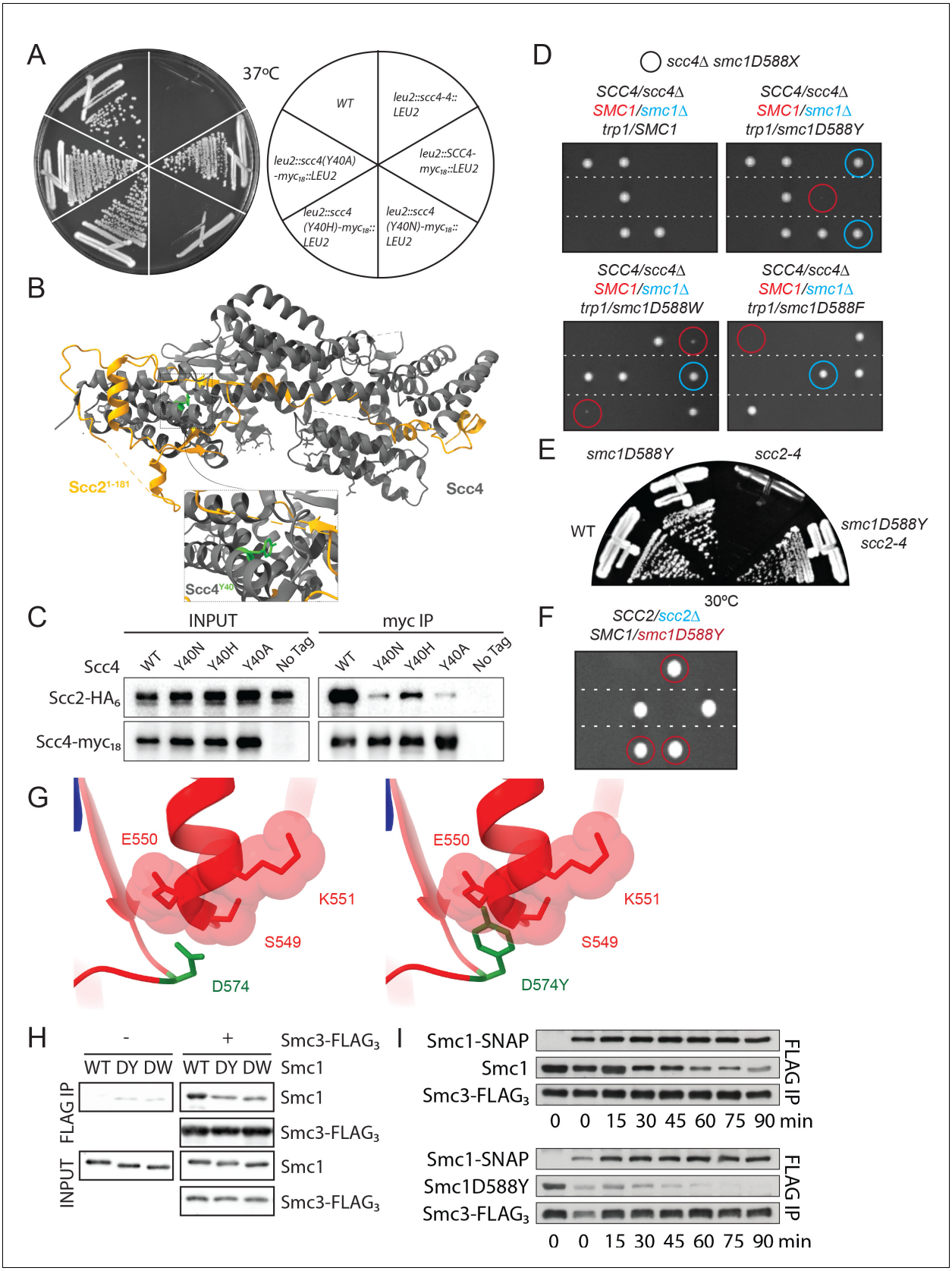

Figure 1—figure supplement 1. A mutation in the hinge domain of Smc1 restores viability in the absence of Scc4. (**A**) Comparison of growth of endogenous *SCC4* with ectopically expressed *SCC4*, *scc4Y40A*, *scc4Y40H*, *scc4Y40N*, and *scc4-4* at 37°C (K7564, K8504, K20350, K20351, K20352,

Figure 1—figure supplement 1 continued on next page

Figure 1—figure supplement 1 continued

K20353). (**B**) Crystal structure of the Scc2$^{1-181}$/Scc4 complex (PDB: 4XDN; ***Hinshaw et al., 2015***). Scc2 is shown in orange, Scc4 in grey, and Scc4Y40 in green. (**C**) Co-immunoprecipitation (co-IP) of wild-type (WT) or mutant Scc4-myc$_{18}$ from cells expressing Scc2-HA6 (K20110, K20111, K20112, K20113, K7564) (**D**) Tetrad dissection performed on heterozygous *smc1Δ/SMC1 scc4Δ/SCC4* strains with *SMC1*, *smc1(D588Y)*, *smc1(D588W)*, or *smc1(D588F)* integrated at the *trp1* locus (K21973, K21974, K22012, K21990). Spores in which *scc4Δ*-related lethality is suppressed by ectopically expressed *smc1* mutants are circled in blue (*smc1Δ*) and red (*SMC1*). Following growth on YPD for 2 days at 30°C, 15.7% of 108 spores contained the markers for *smc1 (D588Y)* and *scc4Δ* (12.0% *smc1Δ*, 3.7% *SMC1*), 27.8% of 72 spores contained the markers for *smc1(D588W)* and *scc4Δ* (18.0% *smc1Δ*, 9.8% *SMC1*), and 5.6% of 72 spores contained the markers for *smc1(D588F)* and *scc4Δ* (4.2% *smc1Δ*, 1.4% *SMC1*). (**E**) Comparison of growth of WT, *smc1D588Y*, *scc2-4*, and *scc2-4 smc1(D588Y)* strains at 30°C (K699, K21416, K5828, K21995). (**F**) Tetrad dissection of a heterozygous *SCC2/scc2Δ* strain in a background heterozygous for suppressor mutation *smc1(D588Y)*. Spores bearing the marker for *smc1(D588Y)* are encircled in red. No spores bearing the marker for *scc2Δ* were detected. (**G**) Graphical D574Y substitution in the structure of the WT cohesin hinge. Y574 adopting the same conformation of D574 crashes with a neighbouring loop (*right*, D574Y). (**H**) Smc1 WT, D588Y (DY) or D588W (DW), and Smc3-FLAG monomeric hinge proteins were mixed in equimolar ratio prior to co-IP with anti-FLAG beads. The amount of protein bound to beads was determined by western blot using anti-HIS antibody to detect SMC proteins. Non-specific binding of Smc1 to anti-FLAG beads is shown in left-hand panels. (**I**) WT Smc1-SNAP competitor was added to Smc1 (WT or D588Y) and Smc3-FLAG preformed heterodimeric hinges, samples were added to BSA-blocked anti-FLAG beads every 15 min for 90 min. Protein bound to beads was detected as in (**E**).

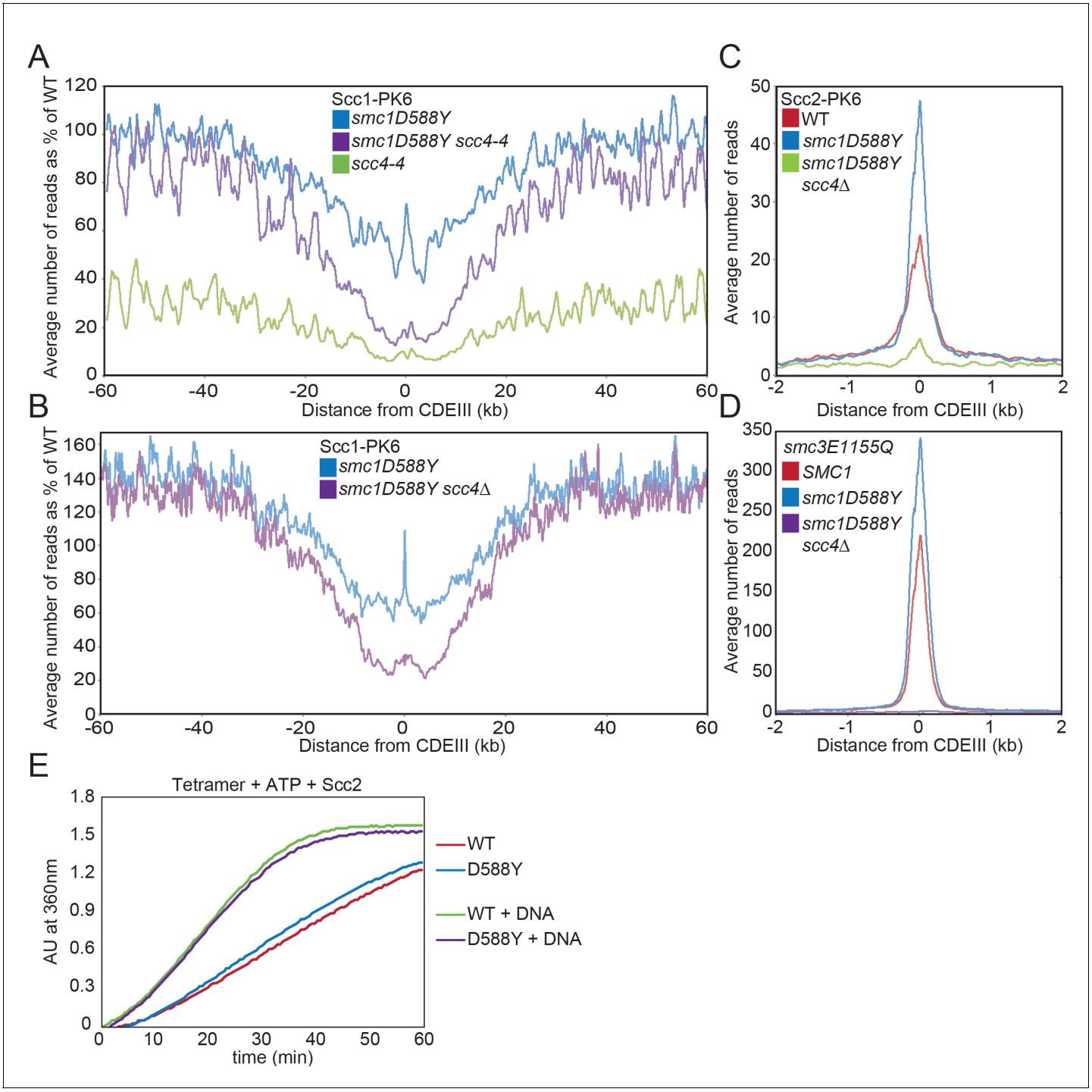

Figure 2. *smc1D588Y* restores cohesin occupancy on chromosome arms in the absence of Scc4. (**A**) Average calibrated ChIP-seq profiles of Scc1-PK6 in *smc1D588Y*, *scc4-4*, and *smc1D588Y scc4-4* cells 60 kb either side of *CDEIII* plotted as a percentage of the average number of reads obtained for wild-type (WT) cells. Cells were pheromone arrested in G1 at 25°C before release at 37°C into medium containing nocodazole. Samples were taken 75 min after release (K22005, K22009, K21999, K22001). (**B**) Average calibrated ChIP-seq profiles of Scc1-PK6 in *smc1D588Y*, and *smc1D588Y scc4Δ* cells 60 kb either side of *CDEIII* plotted as a percentage of the average number of reads obtained for WT cells. Cells were pheromone arrested in G1 at 25°C before release at 25°C into medium containing nocodazole. Samples were taken 60 min after release (K22005, K22009, K19624). (**C**) Average calibrated ChIP-seq profiles of Scc2-PK6 2 kb either side of *CDEIII* in cycling WT, *smc1D588Y*, and *smc1D588Y scc4Δ* cells at 25°C (K21388, K24680, K24678). (**D**) Average calibrated ChIP-seq profiles of ectopically expressed Smc3E1155Q-PK6 2 kb either side of *CDEIII* in cycling WT, *smc1D588Y*, and *smc1D588Y scc4Δ* cells at 25°C (K24562, K24689, K24564). (**E**) ATPase activity of WT or mutant tetramers on addition of ATP and Scc2 in the presence and absence of DNA.

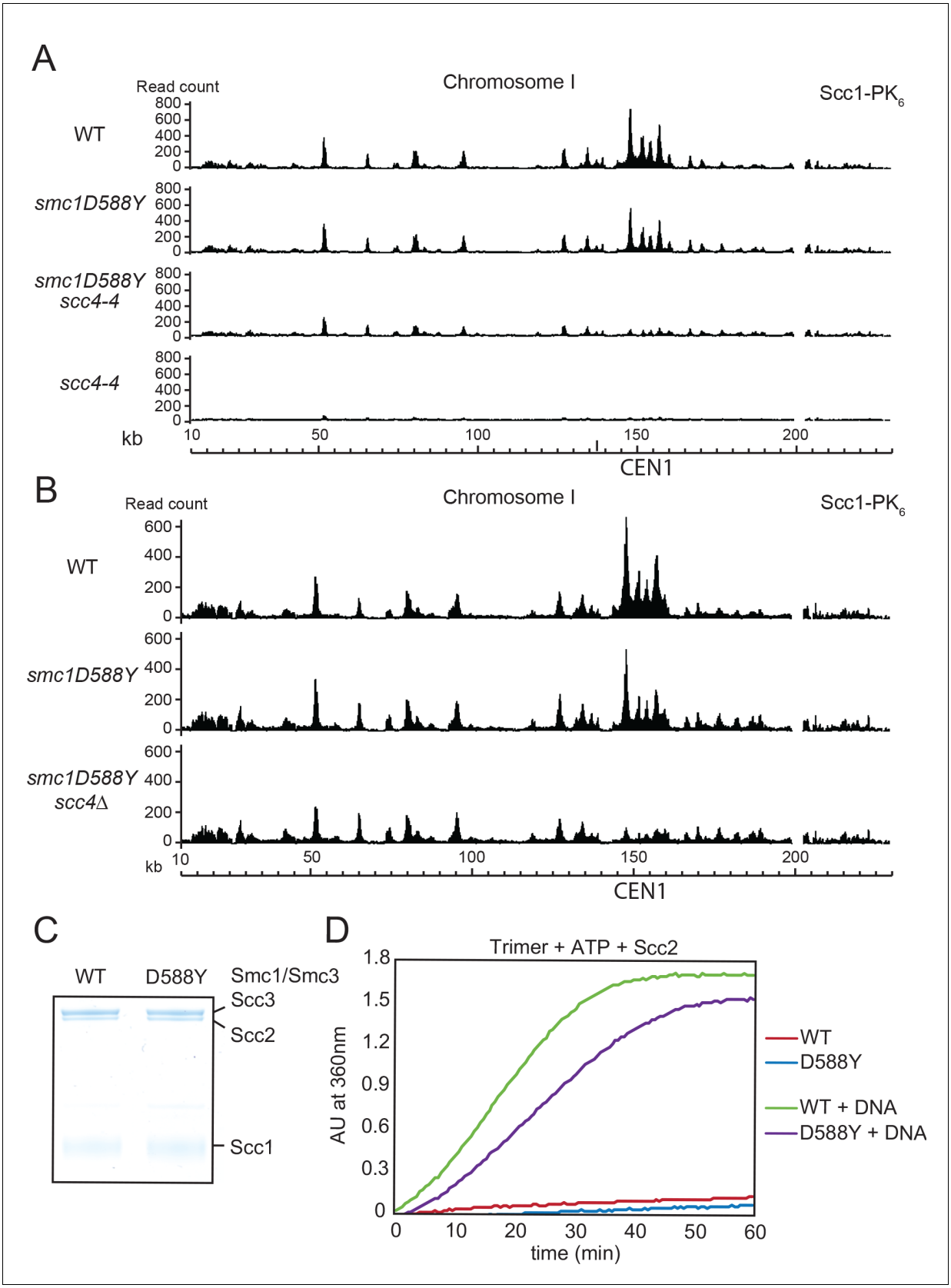

Figure 2—figure supplement 1. *smc1D588Y* restores cohesin occupancy on chromosome arms in the absence of Scc4. (**A**) Calibrated ChIP-seq profiles of Scc1-PK6 in wild-type (WT), *smc1D588Y*, *scc4-4*, and *smc1D588Y scc4-4* cells across chromosome I. Cells were pheromone arrested in G1 at 25˚C

Figure 2—figure supplement 1 continued on next page

Figure 2—figure supplement 1 continued

before release at 37°C into medium containing nocodazole. Samples were taken 75 min after release (K22005, K22009, K21999, K22001). (**B**) Calibrated ChIP-seq profiles of Scc1-PK6 in WT, *smc1D588Y*, and *smc1D588Y scc4Δ* cells across chromosome I. Cells were pheromone arrested in G1 before release into medium containing nocodazole at 25°C. Samples were taken 60 min after release (K22005, K22009, K19624). (**C**) A fraction of the ATPase reaction stained with Coomassie after SDS-PAGE to confirm protein levels. (**D**) ATPase activity of WT or mutant trimers on addition of ATP and Scc2 in the presence or absence of DNA.

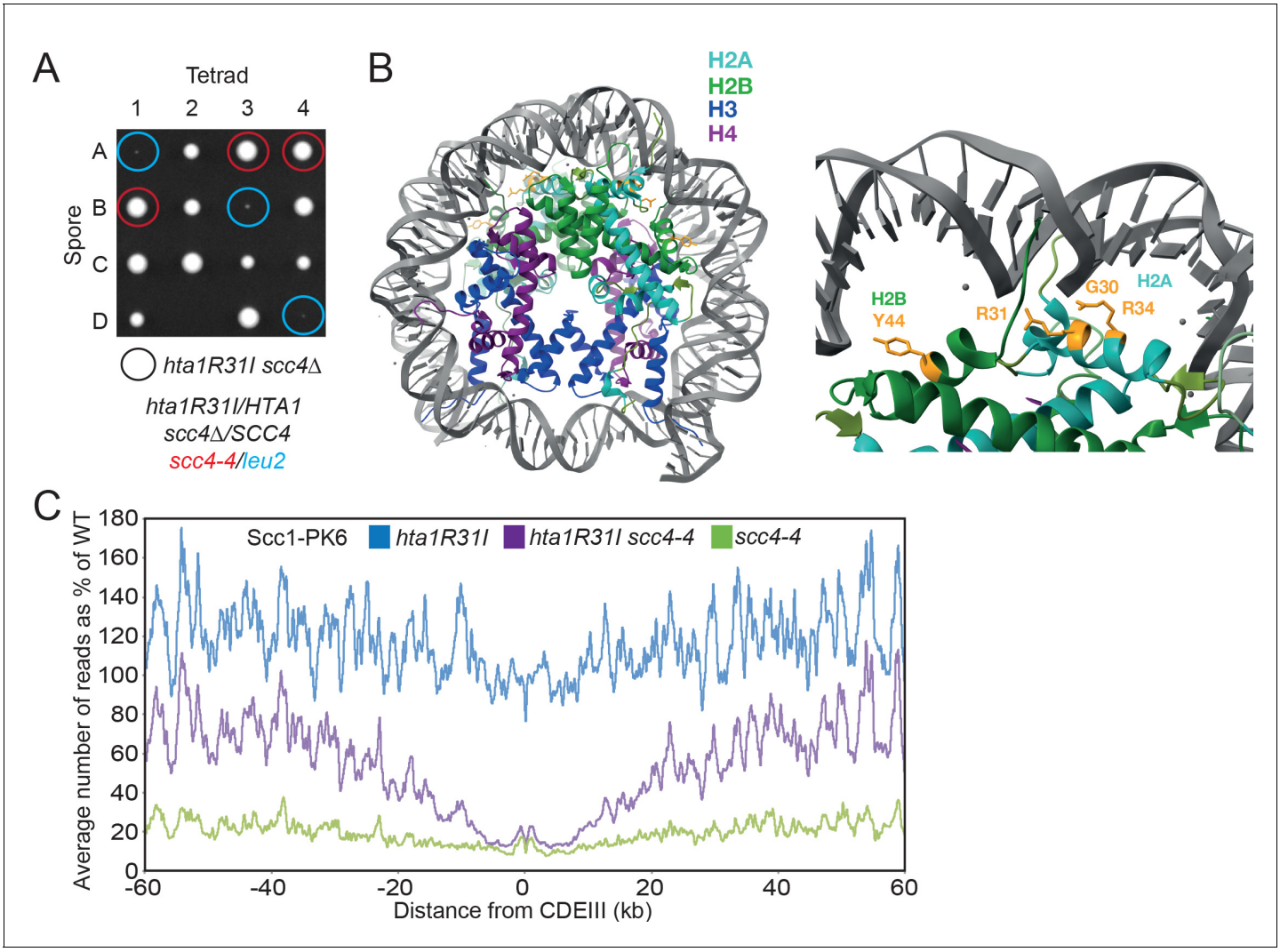

Figure 3. Mutations in *SCC2* and histone genes also suppress *scc4Δ* lethality. (**A**) Tetrad dissection of diploid strains containing *SCC4/scc4Δ leu2/scc4-4 HTA1/hta1R31I*. Spores in which *scc4Δ* is rescued by *hta1R31I* are circled in blue. (**B**) Structure of the yeast nucleosome (PDB: 1ID3; ***White et al., 2001***). H2A is shown in blue and H2B in green. Suppressor mutations are shown in yellow. (**C**) Average calibrated ChIP-seq profiles of Scc1-PK6 in *hta1R31I*, *scc4-4*, and *hta1R31I scc4-4* cells 60 kb either side of *CDEIII* plotted as a percentage of the average number of reads obtained for wild-type (W)T cells. Cells were pheromone arrested in G1 at 25˚C before release at 35.5˚C into medium containing nocodazole. Samples were taken 60 min after release (K22005, K24574, K24568, K22001).

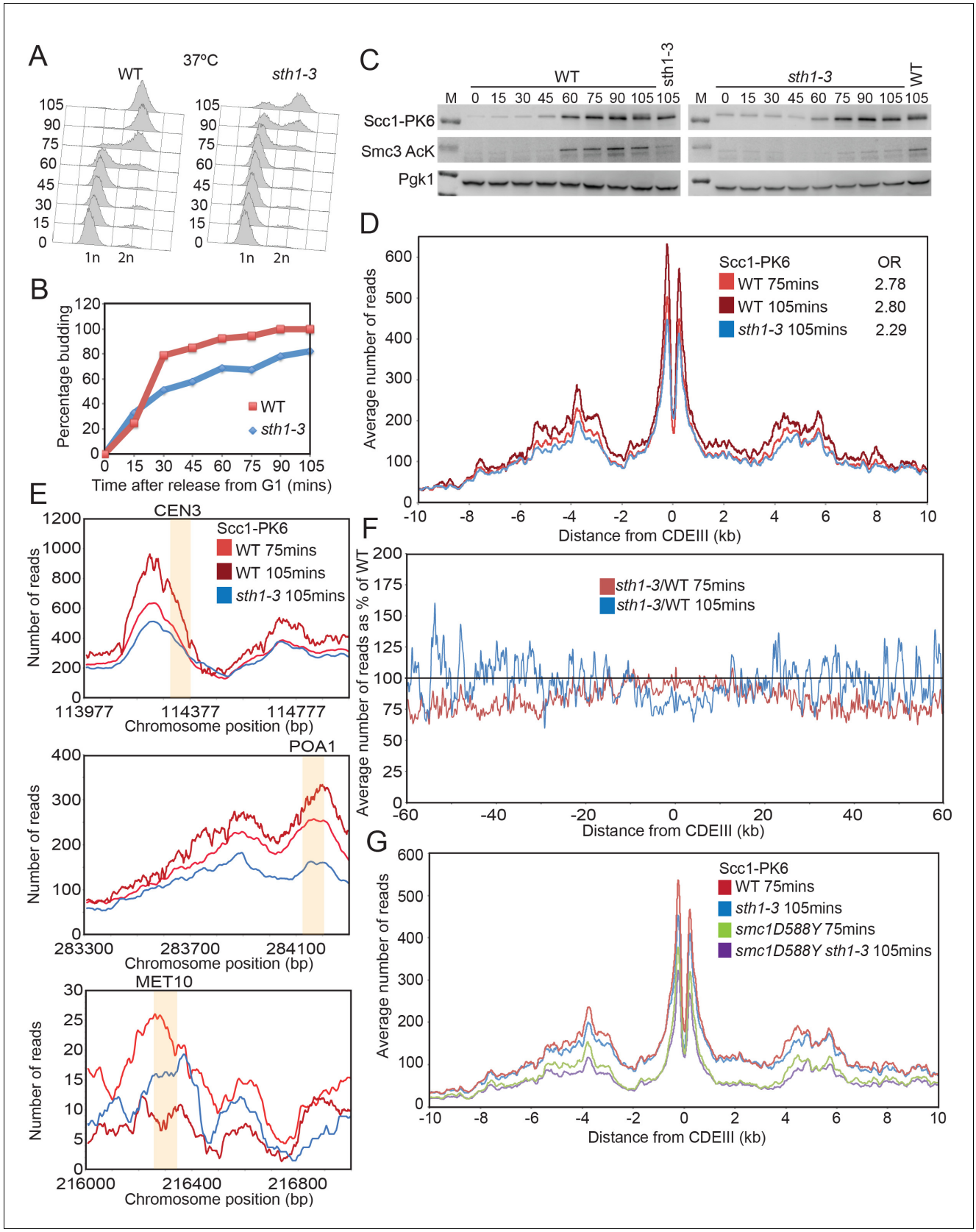

Figure 3—figure supplement 1. Scc4 helps overcome inhibition of loading by nucleosomes. (**A**) Cell cycle progression as measured by FACS of wild-type (WT) and *sth1-3* cells arrested in G1 with pheromone prior to release into nocodazole containing medium at 37°C (K23997, K22005). (**B**) Fraction of

Figure 3—figure supplement 1 continued on next page

Figure 3—figure supplement 1 continued

cells with buds of cells treated as described in (**A**). (**C**) Western blot to measure the levels of Scc1-PK6 and acetylation of Smc3 of cells treated as described in (**A**). (**D**) Average calibrated ChIP-seq profile of Scc1-PK6 10 kb either side of *CDEIII* at 75 min and 105 min after release described in (**A**). The occupancy ratios (OR) were derived as described in ***Hu et al., 2015***. (**E**) ChIP-seq profiles of Scc1-PK6 as in (**D**) at individual loci. Sequences measured in ***Lopez-Serra et al., 2014*** are shaded in orange. (**F**) Average calibrated ChIP-seq profile of Scc1-PK6 in sth1-3 cells at 105 min after release 60 kb either side of *CDEIII* plotted as a percentage of the average number of reads obtained for WT cells at either 75 or 105 min after release. (**G**) Average calibrated ChIP-seq profiles of Scc1-PK6 10 kb either side of *CDEIII* of cells expressing *SMC1* or *smc1D588Y* in the presence of *STH1* or *sth1-3*. Cells were pheromone arrested in G1 at 25˚C prior to release into nocodazole containing medium at 37˚C. Samples were taken at 75 min and 105 min post release, and samples at similar cell cycle stages were compared (K22005, K22009, K23997, K24031).

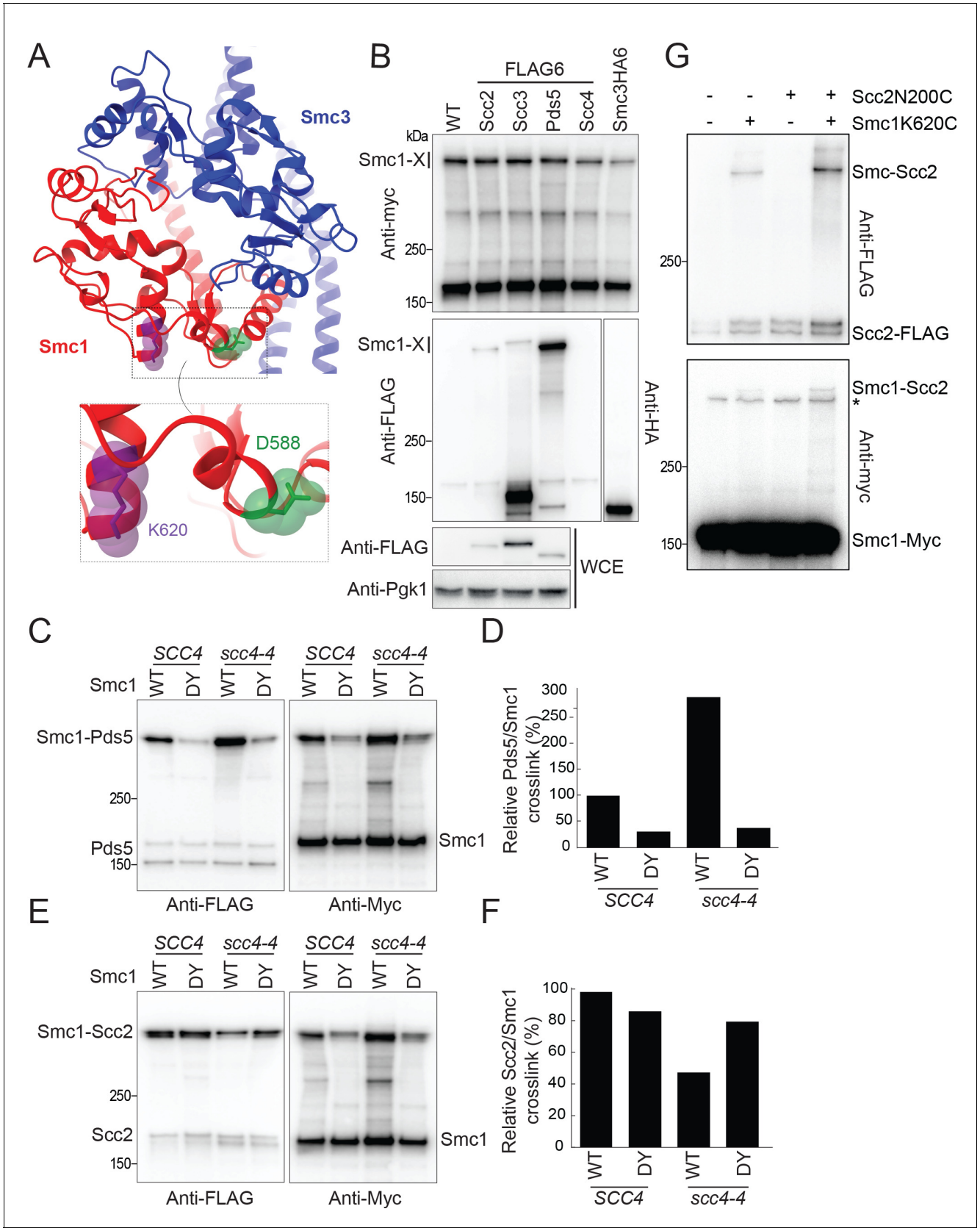

Figure 4. Scc4 regulates an interaction between the hinge domain and HAWKs. (**A**) Modelled structure of the yeast cohesin hinge domain based on bacterial SMC hinge from *Thermotoga maritima* (PDB: 1GXL; ***Haering et al., 2002***). (**B**) Identification of proteins that crosslink to Smc1 hinge. Strains

Figure 4 continued on next page

Figure 4 continued

expressing various cohesin regulators tagged with either FLAG6 or HA6 in combination with Smc1K620BPA-myc were treated with UV prior to immunoprecipitation with PK-tagged Scc1 and the products analysed by western blotting (B1969, B1976, B1983, B2020, B2072, B2079). (**C**) Effect of Scc4 and Smc1D588Y on crosslinking between Pds5 and Smc1 hinge. Cells expressing Smc1K620BPA in the presence or absence of *scc4-4* and Smc1D588Y were exponentially grown at 25˚C and shifted to 35.5˚C for 1 hr. Cells were irradiated with UV, and the cohesin complex was isolated by immunoprecipitation of PK-tagged Scc1. The Myc-tagged Smc1K620BPA was examined by western blot (B2072, B2212, B2214, B2215). (**D**) Quantification of the crosslinks in (**C**) as a percentage of the wild-type (WT) Smc1 crosslinking efficiency. (**E**) Effect of Scc4 and Smc1D588Y on crosslinking between Scc2 and Smc1 hinge. Strains were treated as described in (**C**) (B1969, B2213, B2216, B2217). (**F**) Quantification of the crosslinks in (**E**) as a percentage of the WT Smc1 crosslinking efficiency. The experiments shown in (**C–F**) were performed twice with the same result. (**G**) In vivo cysteine crosslinking of Smc1 hinge with Scc2 protein. Yeast cells expressing Smc1K620C and Scc2N200C were incubated with bismaleimidoethane (BMOE) (B3082, B3107, B3114, and B3116). The crosslinked Smc1/Scc2 was isolated by immunoprecipitation of PK-tagged Scc1 and examined by western blot. * Unspecific crosslink band.

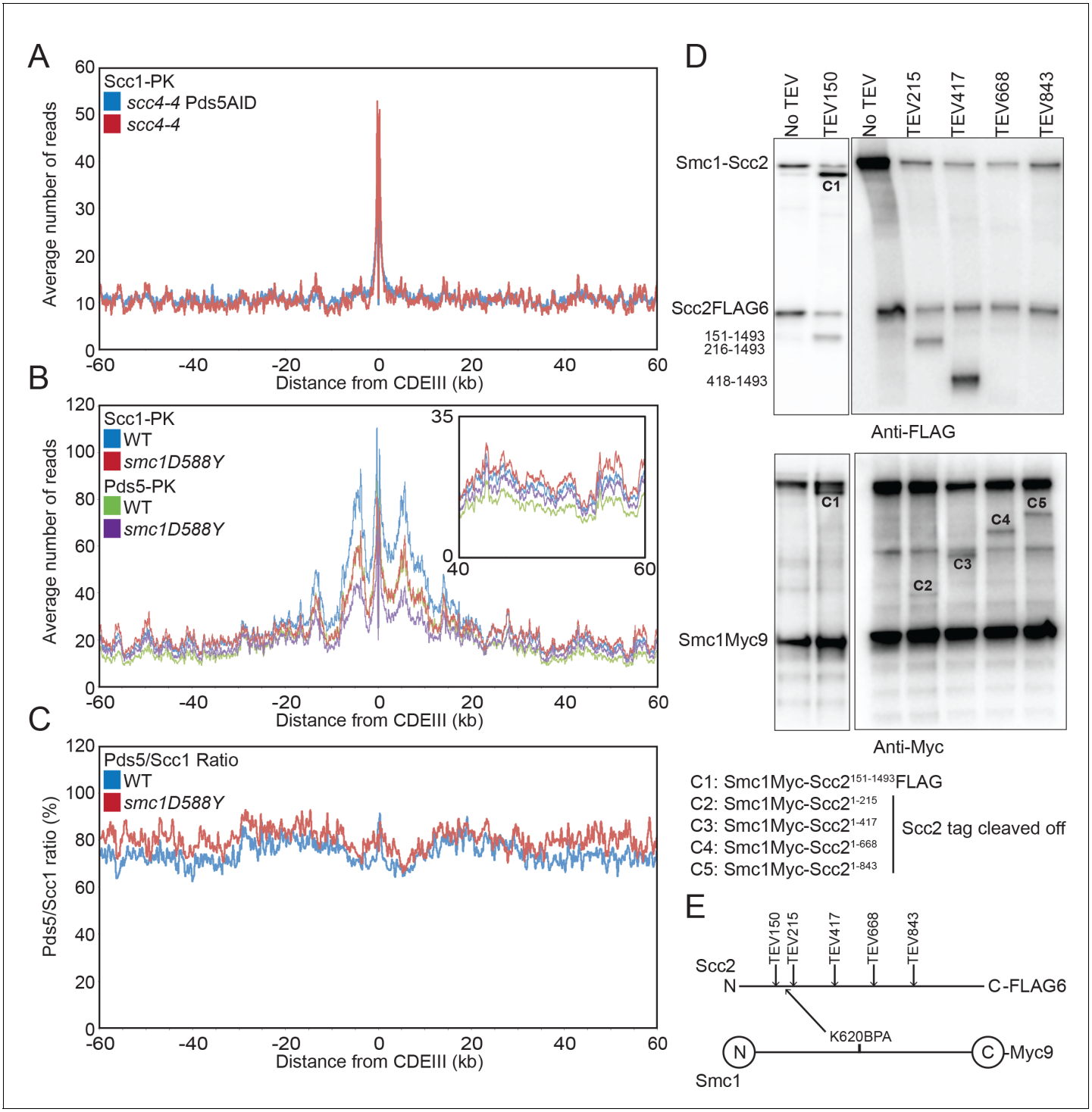

Figure 4—figure supplement 1. Scc4 regulates an interaction between the hinge domain and HAWKs. (**A**) Average calibrated ChIP-seq profiles of Scc1-PK6 60 kb either side of *CDEIII* of cells expressing *scc4-4* in the presence or absence of Pds5-AID. Cells were pheromone arrested in G1 at 25˚C before release at 37˚C into medium containing nocodazole and auxin. Samples were taken 75 min after release (K22001, K27751). (**B**) Average calibrated ChIP-seq profiles of Scc1-PK6 and Pds5-PK6 60 kb either side of *CDEIII* of cycling cells expressing wild-type (WT) or Smc1D588Y. Inset shows magnification of the region 40–60 kb away from *CDEIII* (K19012, K25378, K22005, K22009). (**C**) Data shown in (**B**) plotted as a ratio of Pds5:Scc1 for WT and Smc1D588Y. (**D**) Determination of the Scc2 region crosslinked by Smc1K620BPA. Yeast strains expressing Smc1K620BPA and indicated alleles of TEV-cleavable Scc2 were subjected to UV irradiation (B1969, B2143, B2144, B2145, B2149, and B2298). The crosslink products were co-immunoprecipitated with Scc1-PK and treated with TEV proteinase. The cleaved Scc2/Smc1 crosslinked products were analysed by western blot. (**E**) Schematic of TEV cleavage sites introduced into Scc2 with respect to the crosslink to Smc1K620BPA in (**D**).

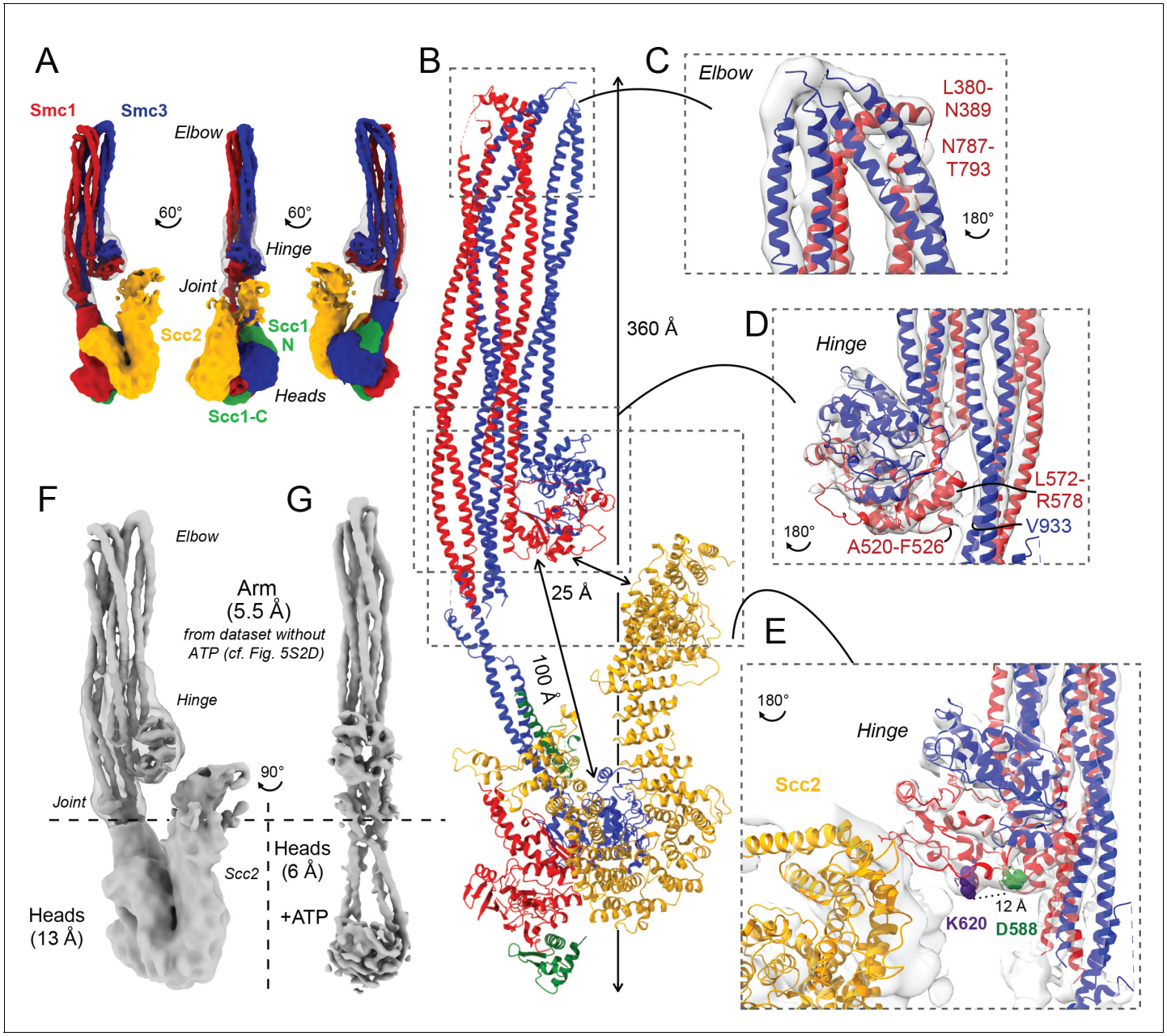

Figure 5. Folded cohesin allows interaction of hinge with Scc2 N-terminus. (**A**) Views of cryo-EM reconstruction of Scc2-bound cohesin coloured by subunit. (**B**) Full pseudo-atomic model of folded cohesin trimer bound to Scc2. (**C**) Close-up of breaks in the coiled coils of Smc3 and Smc1 that constitute the elbow region of cohesin (PDB: 7OGT; EMD-12887). (**D**) Close-up of the interaction between the hinge and Smc3 that stabilises the folded state. (**E**) Close-up of Scc2 N-terminus in proximity of hinge residues K620 and D588Y. (**F**, **G**) Comparison of cryo-EM densities between Scc2-bound and ATP-free cohesin seen in (**F**) (EMD-12880) and ATP-bound cohesin seen in (**G**) (EMD-12889), demonstrating that head engagement is not sufficient for coiled coil unzipping.

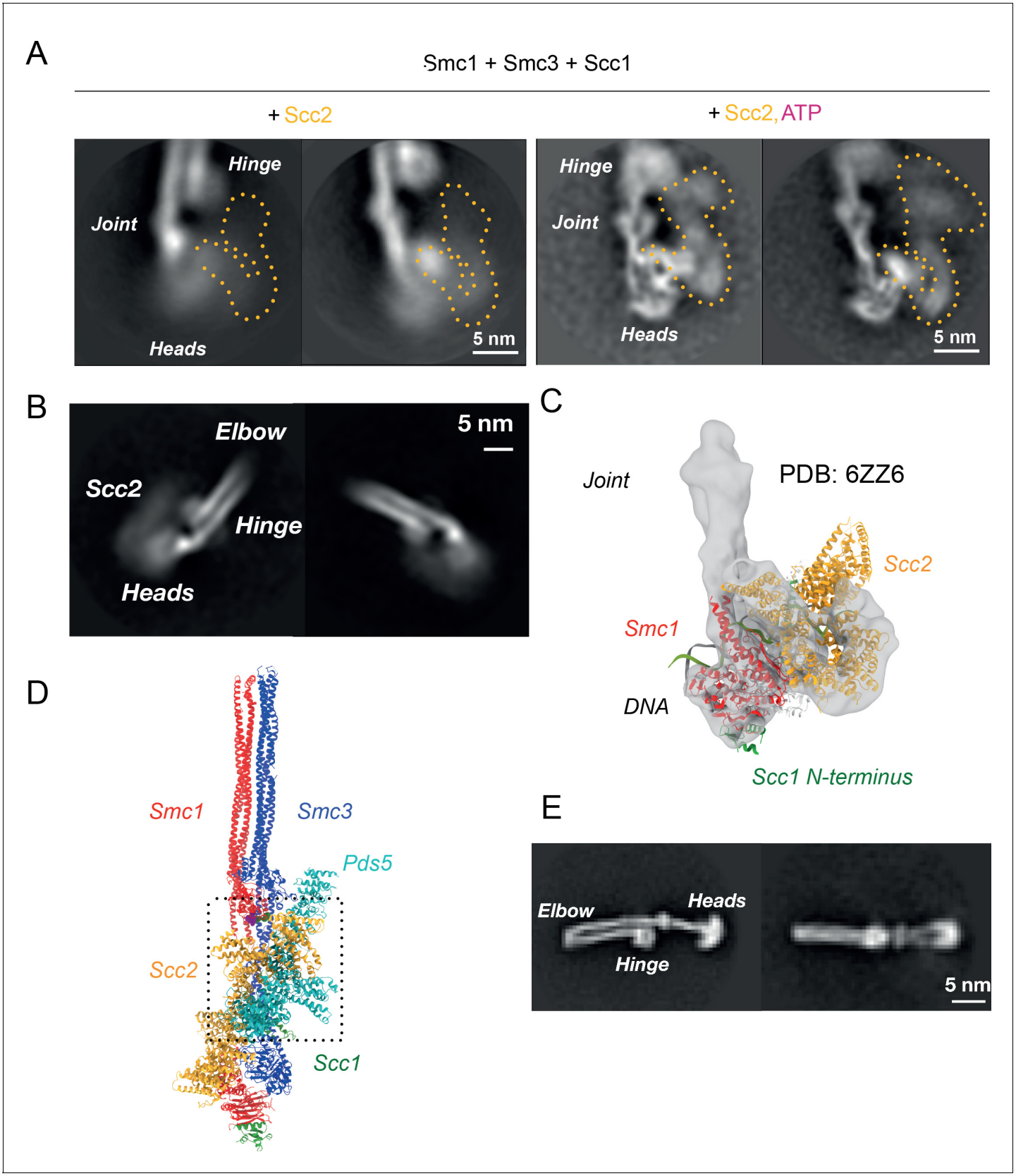

Figure 5—figure supplement 1. Folded cohesin allows interaction of hinge with Scc2 N-terminus. (**A**) 2D classes of Scc2-bound ATPase heads in the absence (left) and presence (right) of ATP demonstrating the stabilising effect of head engagement. (**B**) 2D classes showing flexibility within Scc2 and

Figure 5—figure supplement 1 continued on next page

Figure 5—figure supplement 1 continued

between the heads and the joint. (**C**) Fitting of atomic map from ***Collier et al., 2020*** (6ZZ6) in cryo-EM map made by focused classification. The map originates from the same data as that of ***Figure 5A*** and has been processed to remove the floppy C-terminal head domain of Scc2. (**D**) Overlay of Pds5- and Scc2-bound pseudo-atomic model of cohesin tetramer. The binding of the respective HAWKS is mutually exclusive. (**E**) 2D classes of engaged cohesin in the absence of any HAWKs that demonstrate that folding through the elbow is constitutive.

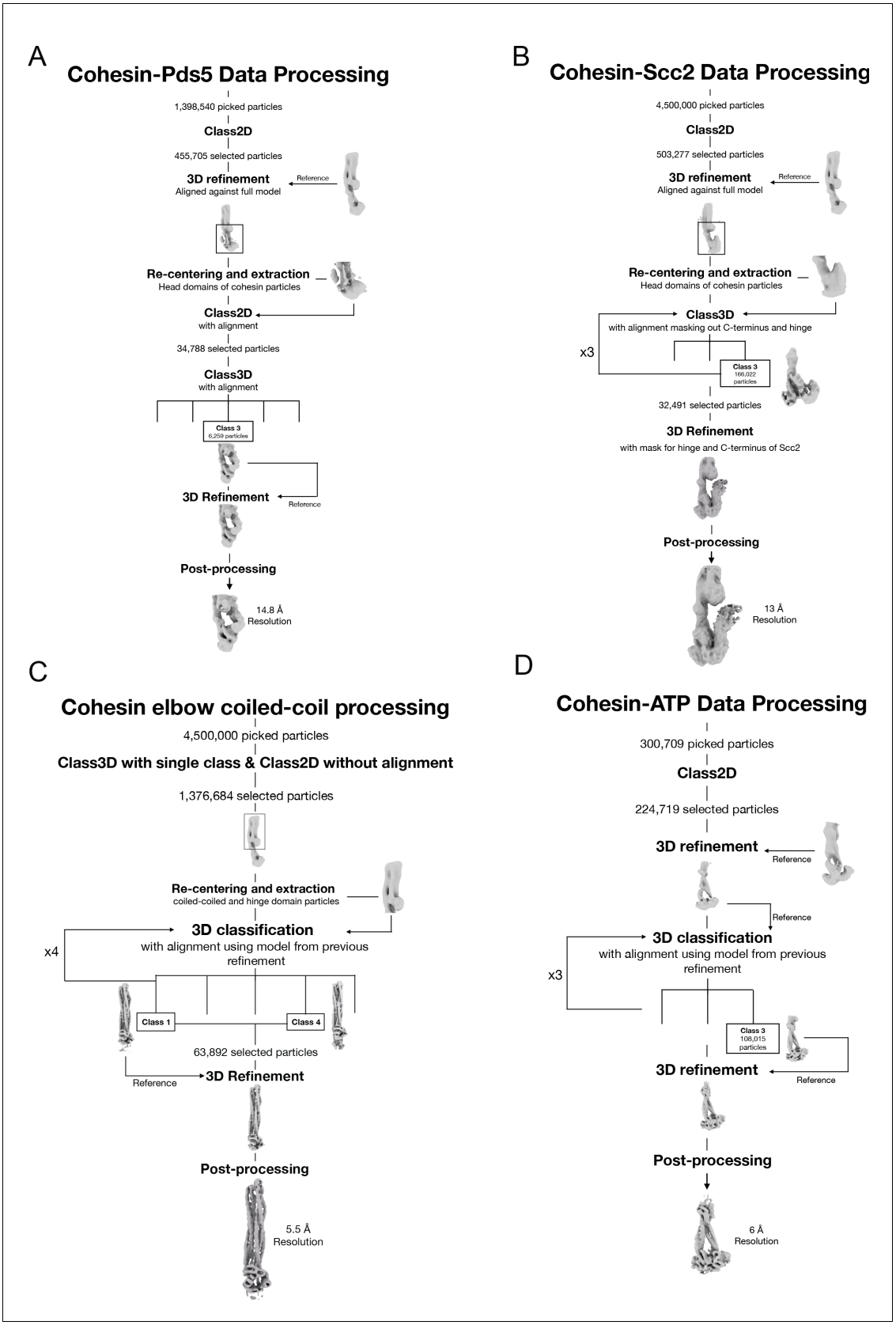

Figure 5—figure supplement 2. Data processing and reconstruction schematics of all cryo-EM maps. Processing workflow to obtain the maps of the folded elbow structure (**A**), the Scc2-bound cohesin complex (**B**), the Pds5-bound cohesin complex (**C**), and the engaged ATPase heads (**D**).

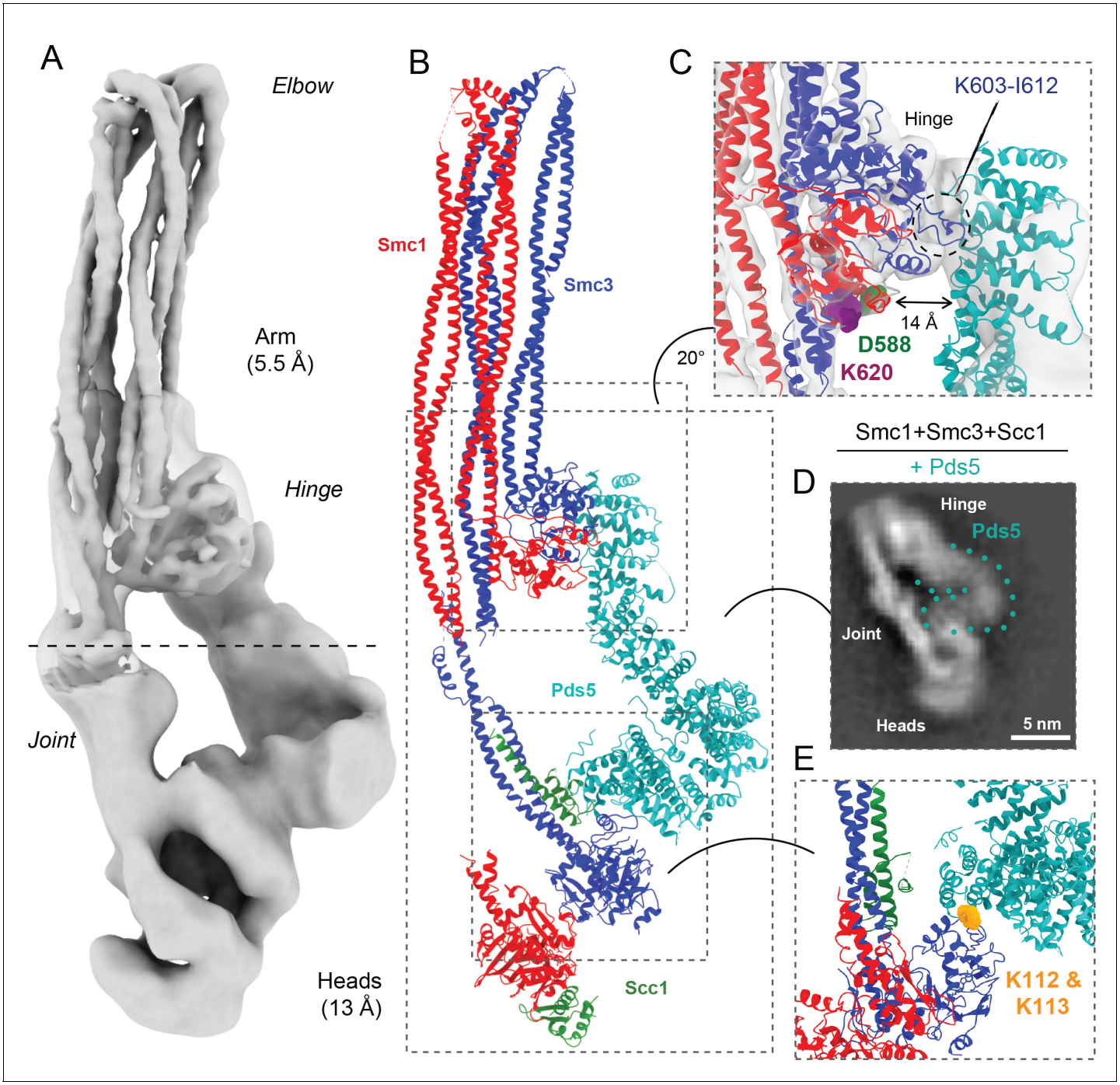

Figure 6. Pds5 binds to Smc3 head while contacting the hinge. (**A**) Composite map of cryo-EM reconstructions of Pds5-bound cohesin (EMD-12888). (**B**) Full pseudo-atomic model of folded cohesin trimer bound to Pds5 coloured by subunit. (**C**) Close-up of interaction between hinge and Pds5 showing proximity of N-terminus of the HAWK to hinge residues D588 and K620. (**D**) 2D classes of Pds5-bound ATPase heads. (**E**) Close-up of Pds5 binding to K112- and K113-proximal region of the Smc3 head.

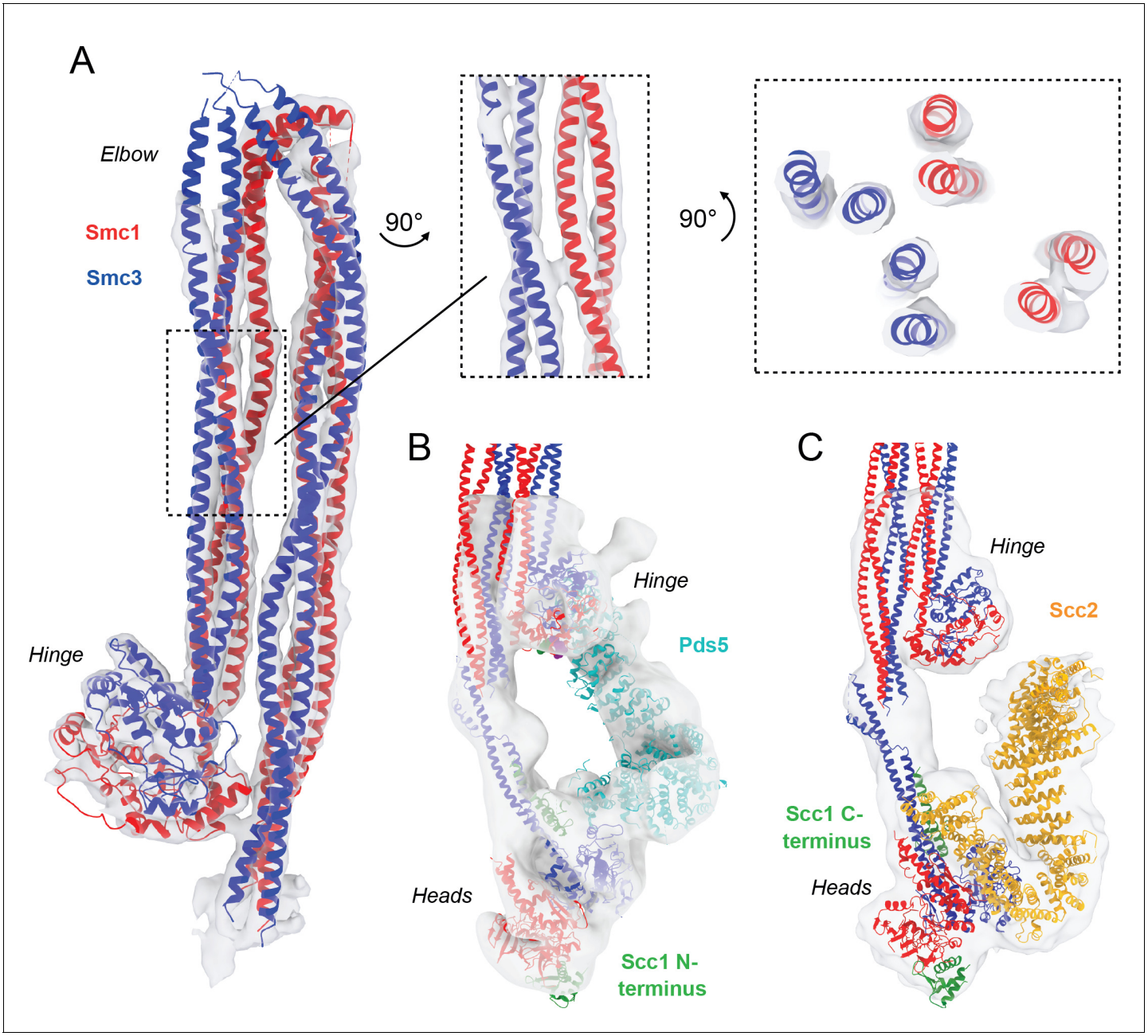

Figure 6—figure supplement 1. Detailed view of fitted atomic structures in cryo-EM maps. (**A**) Coiled coil elbow and hinge pseudo-atomic model fitted into its corresponding cryo-EM density with views of coiled coils from the side and through an intersection. (**B**) Fitting of Pds5 (PDB: 5F0N; ***Lee et al., 2016***), Smc1 (PDB: 1W1W ***Haering et al., 2004***), and Smc3 (PDB: 4UX3; ***Gligoris et al., 2014***) into the Pds5-bound cryo-EM map. (**C**) Fitting of Scc2 (PDB: 5T8V; ***Kikuchi et al., 2016***), Smc1 (PDB: 1W1W; ***Haering et al., 2004***), and Smc3 (PDB: 4UX3; ***Gligoris et al., 2014***) into the Scc2-bound cryo-EM map.

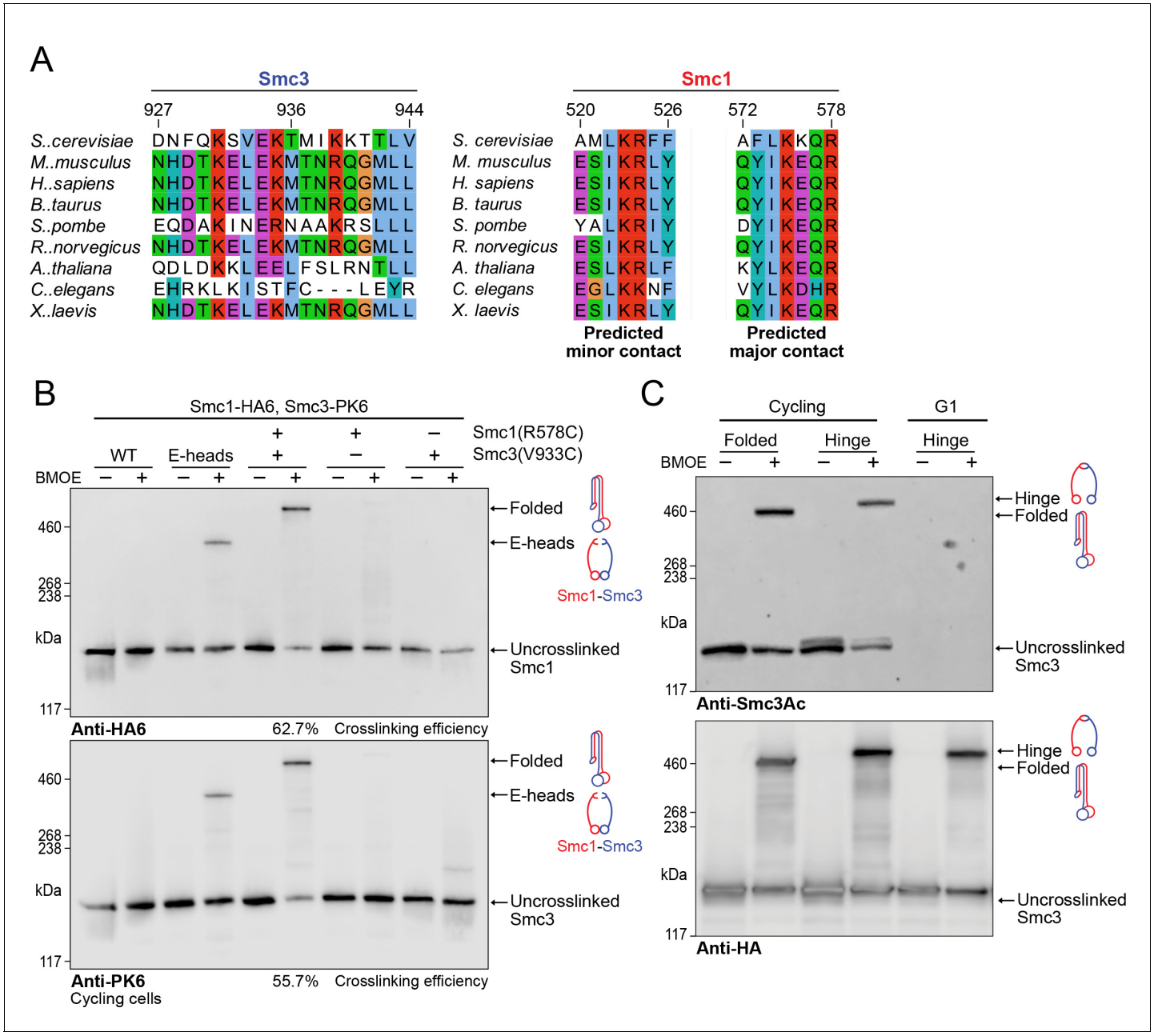

Figure 7. Folding of cohesin's coiled coils occurs in vivo and is a feature of sister chromatid cohesion. (**A**) Sequence conservation analysis for the Smc3 coiled coil and Smc1 hinge helices shown in ***Figure 4D*** shows that the residues are highly conserved. (**B**) Whole-cell extract western blot analysis for the crosslink between Smc1R578C-HA6 and Smc3V933C-PK6 with single cysteine controls probing for hemagglutinin (HA) (top) and PK (bottom). A band shift is observed at the same molecular weight for both blots, confirming the identity of the crosslinked species. Crosslinking of the engaged heads (***Chapard et al., 2019***) was used as a positive control (K28401, K27359, K28585, K28546, K28583). (**C**) Western blot analysis of crosslinking measuring the folded state (Smc1R578C-HA6 and Smc3V933C-PK6) and Smc1-Smc3 hinge dimerisation (***Haering et al., 2008***) probing for acetylated Smc3 (top) and HA (bottom) in logarithmic or pheromone arrested cells (K26081, K28586).